THE ASTROPHYSICAL JOURNAL, 521:179–189, 1999 August 10

ASPHERICAL EXPLOSION MODELS FOR SN 1998bw/GRB 980425

PETER HÖFLICH, J. CRAIG WHEELER, AND LIFAN WANG
Department of Astronomy, University of Texas, Austin, TX 78712;
pah@alla.as.utexas.edu, wheel@alla.as.utexas.edu, lifan@tao.as.utexas.edu
Received 1998 August 7; accepted 1999 March 16

ABSTRACT

The recent discovery of the unusual supernova SN 1998bw and its apparent correlation with the γ-ray burst GRB 980425 has raised new issues concerning both γ-ray bursts and supernovae. Although the spectra of SN 1998bw resemble those of Type Ic supernovae (SNe Ic), there are distinct differences. At early times the expansion velocities inferred by the Doppler shift of (unidentified) absorption features were very high, and SN 1998bw was unusually bright and red at maximum light (Galama et al.). These distinctions make SN 1998bw a candidate of a "hypernova," with explosion energies exceeding normal supernovae by a factor in excess of 10. We present an alternative picture that allows SN 1998bw to have an explosion energy and ejecta mass consistent with core-collapse supernovae, although at the bright end of the typical range. We specifically propose that all SNe Ic are significantly asymmetric and that SN 1998bw is a SN Ic that is distinguished principally by being viewed close to the symmetry axis.

We investigate the hypothesis that SNe Ic and SN 1998bw are the results of aspherical explosions along the rotational axis of basically spherical, nondegenerate C/O cores of massive stars. Light curves for aspherical explosions are computed assuming an ellipsoidal geometry for the ejecta. Guided by the polarization observations of "normal" SN Ic and related events, we assume an axis ratio of 2 near maximum light. The evolution of the isodensity contours with time is discussed. We show that the light curve of SN 1998bw may be understood with an explosion energy of 2×10^{51} ergs, a total ejecta mass of $2\ M_\odot$, and a mass of ^{56}Ni of $0.2\ M_\odot$ if it is observed at a large angle ($\geq 60°$) with respect to the plane of symmetry. In this picture, the high expansion velocities are a direct consequence of an aspherical explosion mechanism which, in turn, produces oblate isodensity contours. Prolate isodensity contours are ruled out. This interpretation suggests that the fundamental core-collapse explosion process itself is strongly asymmetric.

Subject headings: gamma rays: bursts — polarization — radiative transfer — supernovae: individual (SN 1998bw)

1. INTRODUCTION

In the year and a half of great excitement following the discovery of the first optical counterparts of γ-ray bursts, one of the most interesting developments was the detection of the γ-ray burst GRB 980425 by *BeppoSAX* (Boella et al. 1997) and BATSE (Fishman et al. 1993). Because of its correlation in time and location, this γ-ray burst has a high probability of being associated with SN 1998bw (Galama et al. 1998).This connection is supported by the association of a relativistically expanding radio source with SN 1998bw (Kulkarni et al. 1998). From optical spectra, SN 1998bw was classified as a SN Ic by Patat & Piemonte (1998). SNe Ic are commonly attributed to the explosion of the nondegenerate C/O cores of massive stars that have lost their hydrogen-rich and helium-rich layers by the time of the explosion (see e.g., Iwamoto et al. 1994; Clochiatti & Wheeler 1997).

Consistent with typical SNe Ic, the light curve of SN 1998bw showed a fast early rise and reached a peak brightness of 13.6 mag in $V \approx 17$ days after the explosion. After maximum, SN 1998bw showed an exponential decline typical for a supernova light curve but unlike the afterglows that have been observed in other γ-ray bursts. Although the database for SNe Ic is rather sparse, SN 1998bw appears to be unusual. What sets SN 1998bw apart from most of the other observed SNe Ic is the large intrinsic brightness, higher expansion velocities, as indicated by the Si II, Ca H, and Ca K lines (30%–50% higher at maximum light than SN 1994I and SN 1983V; Clochiatti & Wheeler 1997), and an exceptionally bright radio counterpart. For a detailed presentation of the observational data see Galama et al. (1998). In addition, linear polarization has been reported by Kay et al. (1998) at the level of 0.5% on 21 June, about two months after the explosion.

The luminosity of SN 1998bw can be inferred from the redshift of the host galaxy and its reddening. The redshift of the host galaxy ESO 184−G82 is very well known, $z = 0.0085 \pm 0.0002$ (Tinney et al. 1998). The host galaxy is a member of the group DN 193–529 (Duus & Newell 1977). Galama et al. (1998) inferred the Galactic foreground extinction to be $A_V = 0.2$ mag from a combination of *COBE*/DIRBE and *IRAS* maps (Schlegel, Finkbeiner, & Davis 1998). Assuming a Hubble constant of 67 km s^{-1} Mpc^{-1}, the distance can be derived to be 36 Mpc. The main sources of uncertainty in the luminosity determinations are the following: (1) The redshift corresponds to a cosmological expansion v_z of 2550 km s^{-1}. This means the group is not yet fully in the Hubble flow and that peculiar velocities of the group and of the galaxies within the group may be significant, of the order of 10%–20% of the deduced redshift velocity. (2) There is an uncertainty in H_0 of about 10%. (3) Fluctuations in the foreground extinction may be of the order of 0.1 mag, and there may be some extinction is the host galaxy. From (1) and (2), the distance of SN 1998bw, with appropriate uncertainty, can be estimated to be 36 ± 7 Mpc. With the addition of the uncertainty in the reddening, this corresponds to an uncertainty of ± 0.5 mag, or about 60% in the intrinsic brightness.

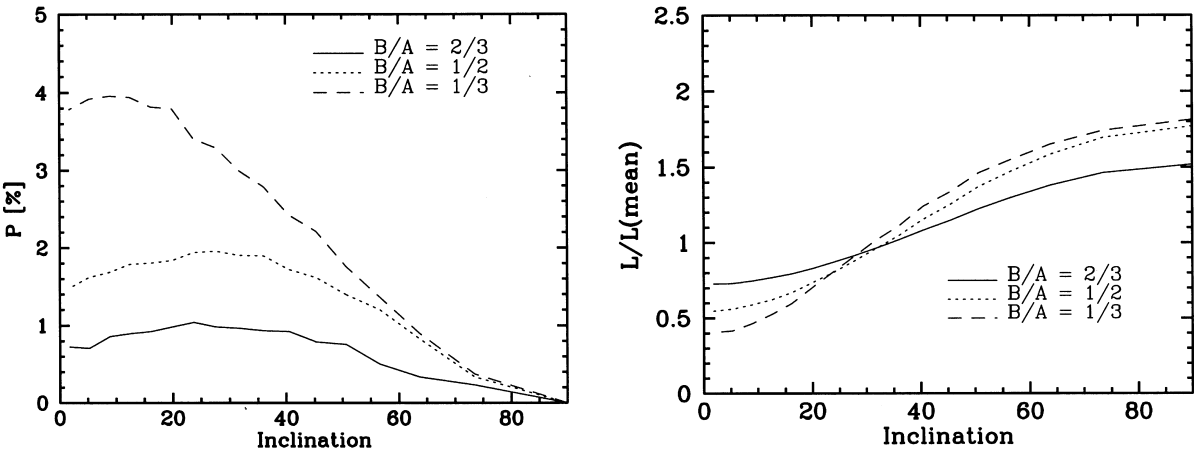

FIG. 1.—Polarization (*left*) and luminosity (*right*) as functions of the angle of the line of sight with respect to the equator are shown for oblate ellipsoids with various axis ratios. The energy source is assumed to be at an optical depth of 5 in Thomson scattering.

Even within this uncertainty, SN 1998bw appeared to be a very luminous event compared to "normal" SNe Ic, favoring the notion that SN 1998bw was a "hypernova" event (Paczyński 1997) with ejected masses and explosion energies at least a factor of 10 larger than other SNe Ic. Based on their light-curve calculations, Iwamoto et al. (1998) found good agreement (better than 0.3 mag over 40 days) with the observed bolometric light curve for models based on the explosion of C/O cores with ejecta masses between 12–15 $M_\odot$, final kinetic energies of $E_{\rm kin} \approx 20$ –50 foe (1 foe = 10^{51} ergs), and the mass of ^{56}Ni between 0.6 and 0.8 $M_\odot$. As noted by the authors, one problem with their calculation may be that the bolometric correction was assumed to be constant with time. Another problem is that the line widths of the synthetic spectra are too narrow by a factor of 2–3 compared to the observations. This indicates that in the models the absorption is formed over too narrow a region in velocity space. This implies that over the phase considered the photosphere in the homologously expanding envelope extends over too narrow a radial region. One interpretation of the narrow theoretical absorption features is that the envelope masses are too large. Woosley, Eastman, & Schmidt (1999) found best agreement with a "hypernova" model that ejects a C/O envelope of about 6 $M_\odot$ with $E_{\rm kin} = 22$ foe and $M_{\rm Ni}$ of 0.5 $M_\odot$. For this model, the bolometric and monochromatic light curves differ from the observations by 0.5–1 mag over the course of 20 days, and all the computed color indices ($B-V$, $V-R$, and $V-I$) are too red by about the same amount. Despite the uncertainties and disagreements in detail, the common denominator of the calculations by Iwamoto et al. (1998) and Woosley et al. (1999) are explosion energies that are larger by a factor of more than 20 and Ni masses that are larger by a factor of 5–10 compared to typical core-collapse supernovae. This clearly points toward the need for a "hypernova" scenario.

Guided by the deduced properties of more traditional core-collapse supernovae and SNe Ic in particular, we seek to demonstrate that an alternative explanation is possible, according to which SN 1998bw falls in the range of "normal" SNe Ic parameters.

Although neutron stars are observed throughout the Galaxy and there is general agreement that SNe II and SNe Ib/c are the results of core collapse, the nature of the explosion mechanism remains unsolved. Both spectral analyses and light-curve calculations support the picture that SNe II, SNe Ib, and SNe Ic may form a sequence involving core collapse within a massive H-rich envelope, within a core that is denuded of most of its hydrogen but retains substantial helium, or within a C/O core that has lost most of its helium, respectively. The analysis of spectra and light curves gives essentially no insight into the geometry of the expanding envelope. It has been demonstrated that, on the level of current spectral fitting, spectra produced in aspherical models can be mimicked by spherical calculations (Höflich et al. 1995). Polarization, however, provides a unique tool to explore asymmetries. As with so many issues, SN 1987A represented a breakthrough in this area by providing the first detailed record of the spectropolarimetric evolution that led to the conclusion that the envelope of SN 1987A was aspherical by about 10% (Méndez et al. 1988; Höflich 1991; Jeffery 1991). In the following years, similar amplitudes of polarization have been observed in a program at McDonald Observatory. These observations continue to confirm the early qualitative conclusion that all SNe II are polarized at about this level (Wang et al. 1996; Wang, Wheeler, & Höflich 1998). There can be a number of reasons why light from a supernova is polarized (Wang et al. 1996, 1998), with an intrinsically strongly aspherical explosion in the core region being only one possibility. There is a trend, however, for the observed polarization to increase in core-collapse supernovae with decreasing envelope mass, e.g., from SN II to SN Ic (Wang et al. 1998). For SN 1993J, in which only a small-mass hydrogen envelope remains, the observed linear polarization was as high as $\approx$1.0%–1.5% (Trammell, Hines, & Wheeler 1993; Tran et al. 1997). For the SN Ic 1997X, the polarization was even higher (Wang & Wheeler 1998). This trend, while tentative, clearly points toward the interpretation that the explosion itself is strongly asymmetric and that this fundamental asymmetry is revealed more clearly as more envelope matter is removed.

From theoretical calculations for scattering-dominated atmospheres, this size of polarization, $\gtrsim$1%, requires axis ratios of the order of 2–3, making these objects highly aspherical. The consequences for the dependence of the apparent luminosity $L(\Theta)$ on the angle Θ of the line of sight has been pointed out and studied in detail (Höflich 1991; 1995a). In Figure 1, we show the dependence of the luminosity and polarization for oblate ellipsoids with axis ratios

between 1.5 and 3 for power-law density profiles $\rho \propto r^{-3}$. In this example, the energy source is assumed to be located at an optical depth of 5. The angular dependence of $L(\Theta)$ changes the apparent luminosity by almost a factor of 4. For a systematic study of the influence of the optical depth, the geometries, the density structure, and the geometry of the envelope, see Höflich (1991, 1995a).

Given the ubiquitous presence of polarization in core-collapse supernovae and SN Ic, inclusion of asphericity effects in SN Ib/c may prove to be critical to their understanding (Wang et al. 1998). The same may be true for SN 1998bw.

In this work, we present a first approach to the problem of asymmetric light curves for SN Ic and SN 1998bw. In the next section, the basic concept and methods are outlined. General results for various geometries are discussed in § 3. In § 4 our results are compared to the observations. A final discussion and conclusions are presented in § 5.

2. DESCRIPTION OF THE CONCEPT AND NUMERICAL METHODS

2.1. *General Concept*

For the initial setup, we use the chemical and density structures of spherical exploding C/O cores of Nomoto & Hashimoto (1988). These structures are scaled homologously to give models of different ejecta mass. This is an approximation, but the details of the chemical profiles are not expected to effect the light curves.

The explosion energy is deposited in the form of thermal energy at the inner edge of this spherical model. The mass cut of the core is adjusted to provide the ejection of the desired ^{56}Ni mass. A problem may be the final distribution of ^{56}Ni, which is fundamentally uncertain in the absence of an understanding of the core-collapse and fallback processes. Possible effects of altering the structure of the ^{56}Ni regions are discussed in § 4. A more important approximation is that we assume that isodensity contours are ellipsoidal. The actual structures resulting from strongly aspherical explosions may be significantly different (see §§ 4 and 5).

Spherical hydrodynamical explosion and the corresponding light curves are calculated first (§ 2.2). Aspherical envelopes are constructed by assuming directionally dependent expansion ratios. An appropriate redistribution of the energy is calculated to construct the aspherical light curve (§ 2.3).

2.2. *The Explosion and Light Curve for Spherical Geometry*

Spherical explosion models are calculated using a one-dimensional radiation hydro code (Höflich, Müller, & Khokhlov 1993; Höflich & Khokhlov 1996) that solves the hydrodynamical equations explicitly by the piecewise parabolic method (Colella & Woodward 1984). The models use 234 depth points. The explosion energy is deposited as thermal energy over the inner 10 depth points.

The spherical code also simultaneously solves for the radiation transport. The radiation-transfer portion of the code consists of (1) an LTE radiation-transfer scheme based on the time-dependent moment equations, which are solved implicitly; (2) a detailed equation of state with an elaborate treatment of the ionization balance and the ionization energies; (3) time-dependent expansion opacities that take into account the composition structure of the explosion model; and (4) a Monte Carlo γ-ray deposition scheme that takes into account all relevant γ-ray transitions and interaction processes (Höflich, Khokhlov, & Müller 1992).

The energy and radiation momentum equations with variable Eddington factors are solved in the comoving frame (Mihalas 1978). The energy equation is solved with appropriately frequency-weighted mean opacities (Höflich et al. 1993). The Rosseland, energy, and Planck mean opacities are obtained from the calculated monochromatic expansion opacities (see below). At each time step, we use $T(r)$ to determine the Eddington factors by solving the frequency-dependent radiation transport equation in the comoving frame in about 100 frequency bands and integrate to obtain the frequency-averaged Eddington factors. We use the latter to iterate the solution with the frequency-integrated energy and flux equations (Höflich, Wheeler, & Thielemann 1998).

In rapidly expanding atmospheres, the opacity, κ_ν, can be significantly enhanced by line-blocking effects as different atomic transitions are Doppler-shifted into the frequency of a propagating photon. Because in supernovae the Doppler shift due to the velocity field is often much larger than the intrinsic line width, the influence of lines on the opacity can be treated quite accurately in the Sobolev approximation (Sobolev 1957; Castor 1974; Höflich 1995b). The corresponding absorption probability is calculated, including bound-bound, bound-free, and free-free opacities based on data for the atomic line transitions from Kurucz & Bell (1995) and Cunto & Mendoza (1992). Typically, frequency-averaged opacities are of the order of 0.05 g cm^{-2}.

Both Thomson scattering with cross section, σ_T, and line scattering are taken into account. For line scattering, an estimate of the fraction of incident photons that are thermalized or otherwise redistributed to other frequencies is crucial. An equivalent two-level formulation for the source function is adopted with parameters determined by comparison with detailed non-LTE (NLTE) calculations that properly take into account the photon redistribution and thermalization processes (Höflich 1995b).

To calculate the monochromatic light curves, we use the $T(r)$ with the time dependence of the structure given by the frequency-integrated solution of the momentum equations. This evolving temperature structure is used to solve the frequency-dependent transfer equations in LTE every 0.5 days. This comoving solution is used to compute L_ν in the observer's frame. The broadband light curves are determined by convolution of L_ν with the filter functions. Here we use a few hundred frequency bands.

2.3. *Light Curves for Aspherical Geometry*

Aspherical density structures are constructed from the spherical density distribution. The simple models presented here are based on the assumption that there is a strongly aspherical explosion in the approximately spherical core. We have not done the actual hydrodynamics to produce such an asymmetric configuration, a task we postpone to future work. Here we impose the asymmetry after the ejecta has reached the homologous expansion phase. Homologous expansion both in one- and two-dimensional geometries can be established if the acceleration is dominated by the early phase of the explosion. From causality, energy and momentum redistribution is limited to a local area determined by the sound speed relative to the expansion speed (in each direction). In core-collapse supernovae, the explo-

sion energy is deposited by the outgoing shock front in the envelope in the form of thermal energy. On timescales of a few hours to days, the thermal pressure accelerates the envelope. During this initial phase, energy and momentum can be redistributed in the envelope on a global scale. Later on, the kinetic energy exceeds the thermal energy by several orders of magnitude. The thermal velocities are about a factor of 1000 smaller than the expansion velocities. Energy and momentum redistribution remains local in mass. The inclination dependence of the kinetic energy thus remains as it is established during the early hydrodynamic phase. Numerical calculations for aspherical explosions of SNe II have confirmed this picture and have shown that the timescales needed establish homologous expansion are of the same order both in one- and two-dimensional geometries and that in two-dimensional geometries the inclination dependence is "frozen out" (Steinmetz & Höflich 1992).

We generate an asymmetric configuration by preserving the mass fraction per steradian from the spherical model but imposing a different law of homologous expansion as a function of the angle Θ from the equatorial plane. By neglecting the actual hydrodynamics, we assume that there is no redistribution of material in the Θ-direction. Note that, for typical density structures, a higher energy deposition along the polar axis results in oblate density structures with prolate Lagrangian surfaces (see below). Such an energy pattern may be produced if jetlike structures are formed during the central core collapse, as suggested by Wang & Wheeler (1998). In contrast, a prolate density structure would be produced if more energy is released in the equatorial region than in the polar direction. Aspherical isodensity structures could also be produced if the original structure were aspherical i.e., if mass were distributed nonuniformly in Θ prior to the explosion compared to a spherical density configuration, by, for instance, rotation. We regard this possibility as less likely to produce large asymmetries since transverse pressure gradients during the explosion will tend to make originally aspherical mass distributions more spherical as the expansion proceeds (Chevalier & Soker 1989).

The initial density structure is spherical, i.e.,

$$\rho(R, \Theta) = \rho(R) , \tag{1}$$

with R being the initial distance of a mass element from the center. To produce aspherical models, homologous expansion of the spherical density distribution is assumed with a scaling that depends on angle, i.e.,

$$\frac{v(R, \Theta)}{R} = C(\Theta) , \tag{2}$$

so that

$$r(\Theta) = C(\Theta)Rt , \tag{3}$$

where t is the time since the explosion and $r(\Theta)$ is the distance of the mass element after time t. For the spherical configuration, $C = v_{\rm sphere}/R$.

Because little is known about the general geometry of the envelopes, we assume ellipsoidal isodensity contours with an axis ratio $E = B/A$ of the photosphere at a reference time, where A is the distance of the photosphere in the x-y (symmetry) plane and B is the distance in the (axial) z-direction. This contour is given by

$$r(\Theta) = r(\Theta = 0)\sqrt{\cos^2 \Theta + E^2 \sin^2 \Theta} . \tag{4}$$

The homology scaling constant, $C(\Theta)$, is then chosen to produce the desired axis ratio starting from the spherical configuration. This means that $C(\Theta)$ has the distribution

$$C(\Theta) = C(\Theta = 0)\left\{\frac{\rho[\tilde{R}(\Theta)]}{\rho[\tilde{R}(\Theta = 0)]}\right\}^{1/3} . \tag{5}$$

Here $\tilde{R}(\Theta)$ denotes the distance from the center of the original spherical model at the beginning of homologous expansion of the mass element that is mapped to angle Θ at the time the isodensity contour is defined. We take this time to be 20 days after the explosion, near maximum light. In our actual calculations, we use equation (5) and do an implicit iteration to determine the functions $\tilde{R}(\Theta)$ and $C(\Theta)$. We note that the solution of equation (5) becomes independent from the time when the homologous expansion is established as long as $R \ll r(20d)$. For power-law density profiles ($\rho \propto r^{-n}$) with $n \neq 3$, the distribution of $C(\Theta)$ with angle would be

$$C(\Theta) = C(\Theta = 0)(\sqrt{\cos^2 \Theta + E^2 \sin^2 \Theta})^{-n/(3-n)} , \tag{6}$$

and that of $\tilde{R}(\Theta)$ would be

$$\tilde{R}(\Theta) = \tilde{R}(\Theta = 0)(\sqrt{\cos^2 \Theta + E^2 \sin^2 \Theta})^{3/(3-n)} . \tag{7}$$

In general, $C(\Theta)$ depends on the underlying density structure as the density gradient (with equivalent local slope $\tilde{n}$) changes between $\tilde{R}(0°)$ and $\tilde{R}(90°)$. In all models discussed here, equation (6) is very close to the exact solution since $\tilde{n}$ varies little over the photosphere. For example, the photosphere is formed around mass fraction 0.45 in our reference model where $\tilde{n}$ is nearly constant (Fig. 2).

The total explosion energy is normalized to that of the corresponding spherical model, i.e.,

$$\int_V \rho(R) v^2_{\rm sphere}(R)\, dV = \int_V \rho(R) v^2(R, \Theta)\, dV , \tag{8}$$

where V is the volume containing the ejecta. This determines $C(\Theta = 0)$. For mean density slopes less than 3, oblate structures are produced if more energy is released in the polar direction. The energy release required to produce an aspherical configuration formally diverges for $n \to 3$.

Because of changes in the density structure, isodensity contours within and beyond the photosphere at day 20 will be nearly, but not exactly, ellipsoidal (see below and Figs. 2, 3, and 4). As the density gradient (or $\tilde{n}$) changes, the axis ratio will change with time and mass coordinate. For the cases discussed in this work, the variations in geometry remain small except in the outer layers in which the photosphere is formed well before maximum light (see below).

We use a Monte Carlo code to compute the light curve of the asymmetric configuration. This code is capable of handling arbitrary three-dimensional geometries, both for the density and the distribution of the sources. The background is assumed to be stationary. In the calculations, the angular space of the emitted photons is discretized by 60 zones in the Θ direction. The extinction, k, opacity, κ, and the emissivity of the photons, η, are assumed to be constant on isodensity contours at each time t. The values of κ, k, and η are taken to be the values of an equivalent mass faction at radius R in the spherical model. The equivalent radius R is defined such that $R = C\langle v\rangle$, where C is the homology constant in the spherical model and $\langle v\rangle$ is the surface-area weighted average of the velocity over the isodensity contour. The values of κ, k, and η on an isodensity contour

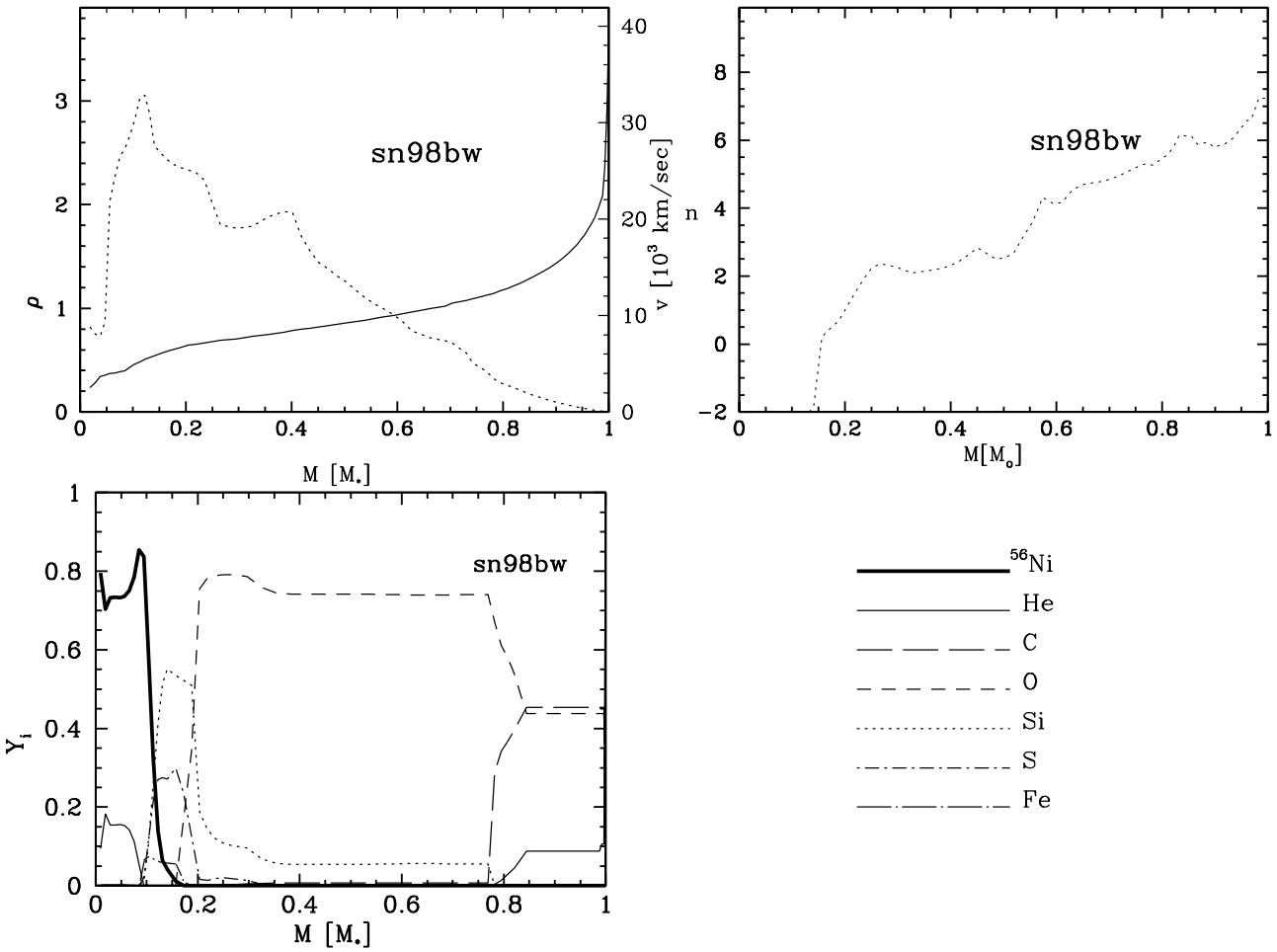

FIG. 2.—Density and velocity structure after the explosion (*upper left*) and chemical structure (*lower left*) as functions of envelope mass. In the upper right plot, the power-law index of the density profile as a function of mass is given. The total mass of the ejecta of our reference model is 2 $M_{\odot}$, and the kinetic energy is 2×10^{51} ergs.

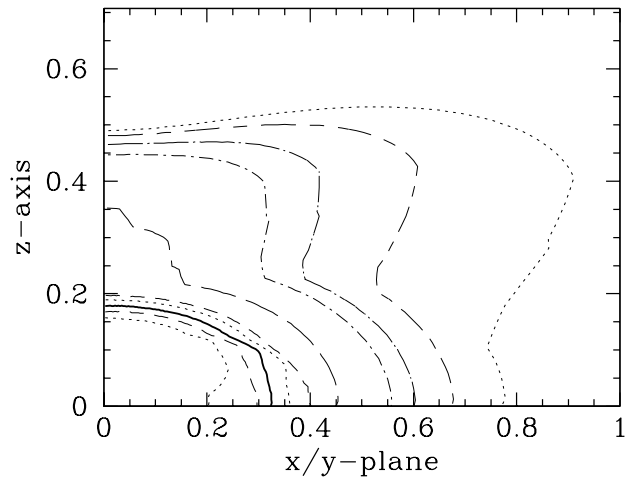

FIG. 3.—Isodensity contours for the reference model with oblate geometry. The contours are defined by the location in the equatorial plane of mass elements that correspond to mass fractions in the spherical model of 0.1, 0.3, 0.5 (*thick line*), 0.6, 0.7, 0.8, 0.9, 0.93, 0.96, and 0.98. The isovelocity contours are spheres, and Lagrangian mass elements are prolate as given by eqs. (5) and (6).

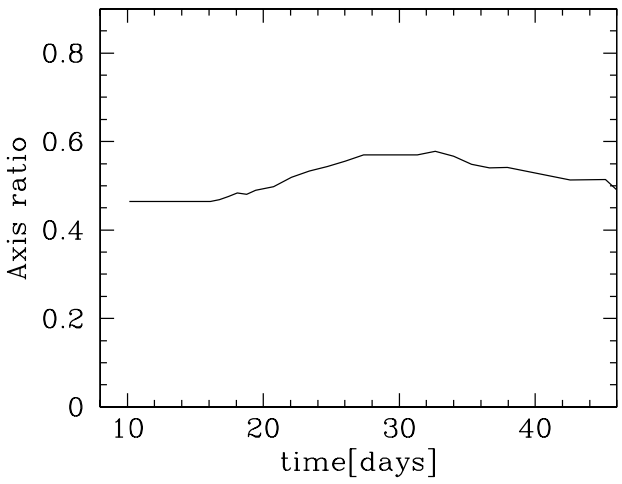

FIG. 4.—Axis ratio of the isodensity contour at the photosphere ($\tau_{\text{scattering}}$, $\Theta = 0 = 0.667$) for the oblate ellipsoid is given as a function of time for the reference model with oblate geometry. The axis ratio varies with time because the power-law index n varies with depth.

are thus given by

$$\kappa[\bar{R}(r, \Theta, t), t] = \kappa_{\rm sphere}(R, t) , \quad (9)$$

$$k[\bar{R}(r, \Theta, t), t] = k_{\rm sphere}(R, t) , \quad (10)$$

and

$$\eta[\bar{R}(r, \Theta, t), t] = \eta_{\rm sphere}(R, t) , \quad (11)$$

where $\bar{R}(r, \Theta, t)$ is the general mapping function of mass elements from the spherical model to respective isodensity contours, e.g., $\tilde{R}(\Theta) = \bar{R}(r_{\rm photosphere}, \Theta, 20$ days). Here we take the local quantities from a representative mass element of the spherical model. Note that the mass elements on the isodensity contours arise from different depths in the original spherical model with varying k, κ, and η. This forbids a direct mapping of the properties of the Lagrangian mass elements because it would strongly violate the energy balance between absorption and emission. The prescription of equations (9)–(11), in which k, κ, and η are chosen from a single depth in the original spherical model, although an approximation, preserves the balance of absorption and emission from the original spherical model.

Photons are generated in the Monte Carlo code in proportion to η. The result of the Monte Carlo calculation is the relative distribution of the luminosity as a function of angle and time, $l(\Theta, t)$. The influence of the distribution functions of the photon sources, η, for various density structures has been studied in detail (Höflich 1991). From these studies, errors in $l(\Theta, t)$ are be expected to be $\approx 10\%$. For more details, see Höflich (1991, 1995a) and Höflich et al. (1995). The bolometric and broadband light curves are constructed by multiplication of the spherical light curves at each time step by the redistribution factors $l(\Theta, t)$ calculated by the Monte Carlo code, i.e.,

$$L_{{\rm bol}, BVRI}(\Theta, t) = l(\Theta, t) L_{{\rm bol}, BVRI}({\rm mean}) , \quad (12)$$

where $L_{{\rm bol}, BVRI}({\rm mean})$ stands for the bolometric and $BVRI$ light curves for spherical geometry.

The axis ratio of the isodensity contours at the photosphere varies rather slowly in time (see below, § 3, Fig. 4). Therefore, to first order, variations of the geometry of the envelope can be neglected over the diffusion timescale of a photon. Typical conditions at the photosphere and therefore the colors are expected to be similar in both the spherical and aspherical models. For an oblate ellipsoid with an axis ratio of 2, the area seen pole-on is about twice as large as the area of the corresponding spherical structure, and the value of $L/L({\rm mean})$ observed along the symmetry axis is also about 2 (see Fig. 1), so the flux is about the same. Quantitatively, the energy flux $F(\Theta)$ is found to be similar in the spherical and aspherical configurations to within $\approx 40\%$. To first order (Wien's limit), a change of $F(\Theta)$ by 40% corresponds to a change in color indices by about 0.1 mag.

Equation 12 contains the implicit assumption that the mean diffusion times are the same for spherical and aspherical envelopes. In reality, the diffusion timescale will be shorter for aspherical configurations because at a given mass element the diffusion time varies as r^{-4} because of its quadratic dependence on the optical depth, whereas the density goes as r^{-3}. The change in the diffusion timescale mostly effects the very early phases of the light curve when the diffusion timescale is much longer than the expansion timescales. During the initial rise, the luminosity will be underestimated (see § 4). This represents another approximation that is consistent with these trial calculations but inadequate for a full understanding of the radiative transfer in asymmetric configurations. We intend to do full aspherical radiation hydro calculations that will eliminate this mapping process.

All models in the next section are constructed in such a way that at day 20 the axis ratio at the photosphere is 0.5 and 2.0 for oblate and prolate ellipsoids, respectively. The photosphere is defined at the density at which the optical depth in Thomson scattering equals $\frac{2}{3}$ in the spherical model. In comparison to the spherical model, the expansion parameters are a factor of ≈ 2.2 larger along the pole for oblate ellipsoids and a factor of ≈ 1.5 larger for prolate ellipsoids along the equator.

3. RESULTS

We first calculated aspherical light curves based on C/O cores with initial total masses of 1.8 and 2.1 $M_\odot$ (models CO18 and CO21) that have ejecta masses of 0.5–0.8 $M_\odot$ (CO18 and CO21, respectively), that have explosion energies of $E_{\rm kin} = 10^{51}$ ergs, and that eject ≈ 0.07–0.08 $M_\odot$ of ^{56}Ni. In previous work, model CO21 was found to give a good representation of the $BVRI$ light curves of the SN Ic 1994I (Iwamoto et al. 1994). This first set of models failed to represent SN 1998bw in several respects. The luminosity is increased by about a factor of 2 in the polar direction for the oblate model and about a factor of 1.5 in the equatorial plane for the prolate model. Despite this boost in the luminosity, these models are too dim even within the uncertainties discussed in the introduction. The maximum was also too early by about 5 days. Finally, these models are very blue at maximum light. An increase of the asphericity does not solve these problems (see Fig. 1).

To boost the total luminosity to the level of the observations, we increased the amount of ejected ^{56}Ni to 0.2 $M_\odot$. This quantity of nickel is still below the estimate of 0.3 $M_\odot$ in SN 1992, which is the most luminous SN II event observed so far (Schmidt et al. 1997), and substantially less than in the "hypernova" models of Iwamoto et al. (1998) and Woosley et al. (1999). The time of maximum light is rather insensitive to asphericity effects (Figs. 7 and 8). In principle, the rise time could be increased by an increase in mass or, alternatively, by a decrease in the expansion rate. The latter option can be ruled out because of the need for large expansion velocities. The need to delay the time to maximum therefore suggested the need to increase the ejecta mass with an appropriate increase in the kinetic energy to provide the observed expansion.

We thus computed a series of models with $M_{\rm ej} = 2\ M_\odot$, $E_{\rm kin} = 2 \times 10^{51}$ ergs, and $M_{\rm Ni} = 0.2\ M_\odot$. The chemical structure and the final density structure during the phase of homologous expansion are given in Figure 2. The escape probability for γ-rays from the radioactive decay of ^{56}Ni and ^{56}Co increases rapidly after maximum light (Fig. 5), with consequences as discussed below.

For illustration, the isodensity contours are given for the oblate structure in Figure 3. They are close to elliptical except for the very outer layers. Note that the shape of the photosphere and the corresponding change in the polarization early on provides a sensitive tool for studying details of the asphericity in the distribution of the explosion energy.

The density slope at the photosphere changes with time. This causes the axis ratio at the photosphere to vary. As an

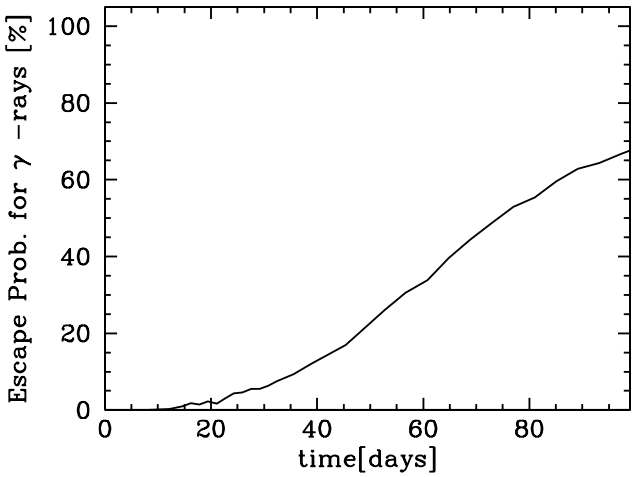

FIG. 5.—Escape probability for γ-rays as a function of time for the model of Fig. 2.

example, we give the time evolution of the oblate ellipsoid axis ratio in Figure 5. The envelope becomes transparent at about day 70.

In Figure 6, $L(\Theta)$ is given for oblate and prolate ellipsoids. Asphericity of the amplitude we have assumed here can change the luminosity over a range of roughly 2 magnitudes, depending on the line of sight. For oblate ellipsoids, the luminosity is enhanced pole-on, whereas for prolate structures the enhancement occurs in the equatorial direction. Combined with the polarization properties, this provides a clear separation between oblate and prolate geometries. The linear polarization P always goes to zero if the structure is seen pole-on, and P increases for lower latitudes (Höflich 1991). Statistically, for oblate density structures we thus expect that high apparent luminosity will be associated with low polarization and low luminosity will be associated with high polarization. The opposite trend is expected for prolate geometries. The maximum amplification of L is larger in oblate structures compared to prolate configurations because of the differences in the projected area for a given axis ratio.

Observations of the polarization of SN 1998bw 23 days after the explosion show little polarization ($\leq 1\%$; Patat & Piemonte 1998). By day 58, the intrinsic polarization was reported to be 0.5% (Kay et al. 1998). Polarization data on SNe Ic are rare, but this value is less than observed in SN 1993J and in SN Ic 1997X (Wang et al. 1998; Wang & Wheeler 1998). SN 1998bw was also rather bright. The polarization is time dependent, and we do not necessarily know the maximum value in SN 1998bw. Nevertheless, the

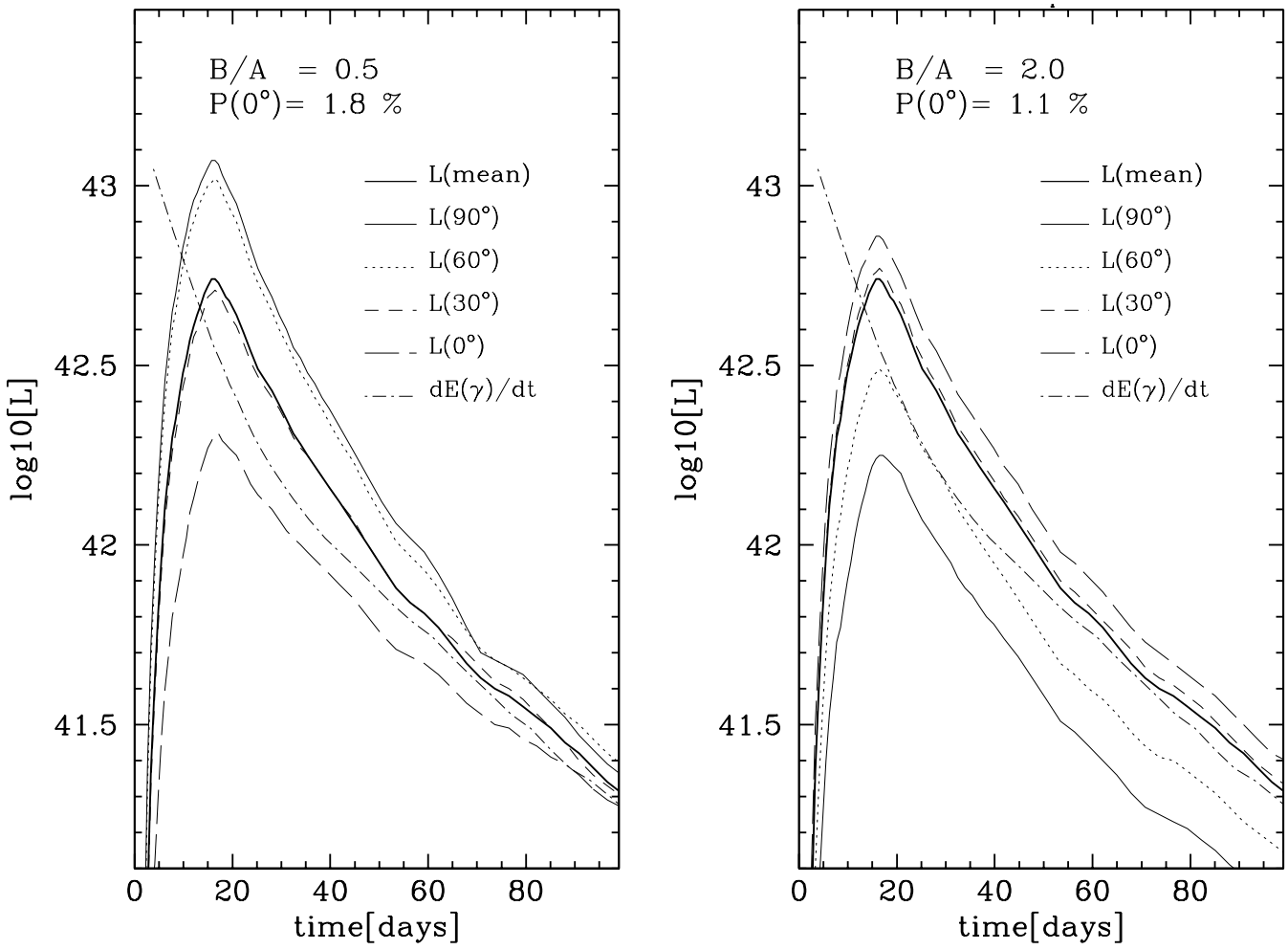

FIG. 6.—Directional dependence of the bolometric light curve for oblate (*left*) and prolate (*right*) ellipsoids for the reference model. The luminosity of the corresponding spherical model is shown as L(mean). In addition, the instantaneous γ-ray deposition is shown. $P(0^\circ)$ is the polarization at maximum light [$P(\Theta) \approx P(0^\circ) \times \cos^2 \Theta$].

evidence suggests that, if asymmetry is involved, oblate geometries are to be favored over prolate geometries. We therefore concentrate on oblate structures in the following.

The corresponding broadband light curves for the oblate geometry are shown in Figure 7. The absolute magnitude of our model with $M_{ej} = 2\ M_\odot$, $E_{kin} = 2 \times 10^{51}$ ergs, and $M_{Ni} = 0.2\ M_\odot$ can be as high as -19.0, -19.3, -19.4, and -19.5 mag in B, V, R, and I, respectively, when viewed pole-on. The decline rate tends to decrease from the IR to B.

4. THEORY VERSUS OBSERVATIONS

For the comparison between the observed and theoretical light curves, we assumed an interstellar extinction $A_V = 0.2$ and a distance of 36 Mpc. We have used the relative calibration of Woosley et al. (1999) for the "bolometric light curve" that was obtained by integrating over the $UBVRI$ photometry. The broadband data were obtained from Galama et al. (1998). In the following, it should be remembered that the absolute calibration of the light curve is uncertain by a factor of $\pm 60\%$, as shown in the introduction.

The comparison of the model and observed bolometric light curve in Figure 8 shows that for our model, SN 1998bw must be observed from an angle of $\geq 60^\circ$ from the equator. The same conclusion can be tentatively drawn from the relatively small size of the linear polarization observed. Within the framework of our approach, any prolate density structure can be ruled out. The required boost in the luminosity by a prolate geometry would require even larger asphericities, but the required asphericity would imply linear polarization of several percent (Höflich 1991).

Overall, the broadband light curves agree with the data within the uncertainties expected from our approximations. In particular, the time of maximum agrees within 2 days except in the I band. The observed color is $B-V = 0.47$ at maximum. The intrinsic color excess $B-V$ corrected for reddening matches the observations within 0.1 mag at maximum. After the initial rise of ≈ 7 days, the agreement in the colors is better than 0.3 mag over the epoch modeled. The main discrepancy with the observations occurs during the first week of the rise when our models are too dim. During this phase, the diffusion timescales are much longer than the expansion time. Under these conditions, our approximation of redistribution of the energy of a spherical model to the ellipsoidal configuration breaks down. Qualitatively and compared to a spherical model, the increased expansion rate coupled with the larger surface area in aspherical configurations will cause a faster release of stored energy and may cause a steeper rise of the early light curves. In addition, clumpiness in the ejecta can reduce the discrepancy between the theoretical and observed light curves. One possible effect is that clumps of radioactive nickel could be mixed outward and thus heat the outer layers, leading to an increased brightness at early times, but also perhaps to some later change in color. Secondly, if the overall material

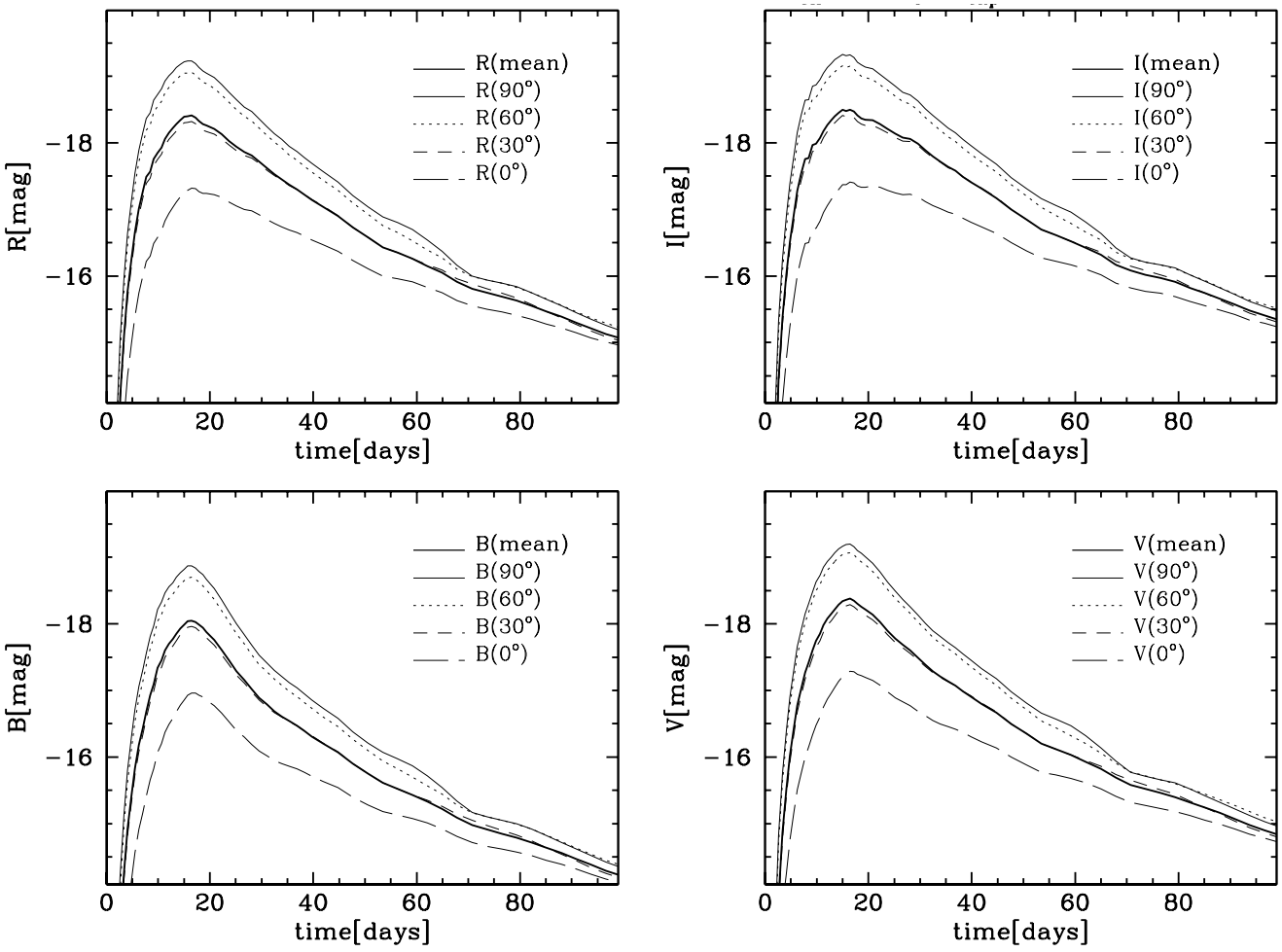

FIG. 7.—Same as in Fig. 6, but for the broadband light curves and the oblate geometry only

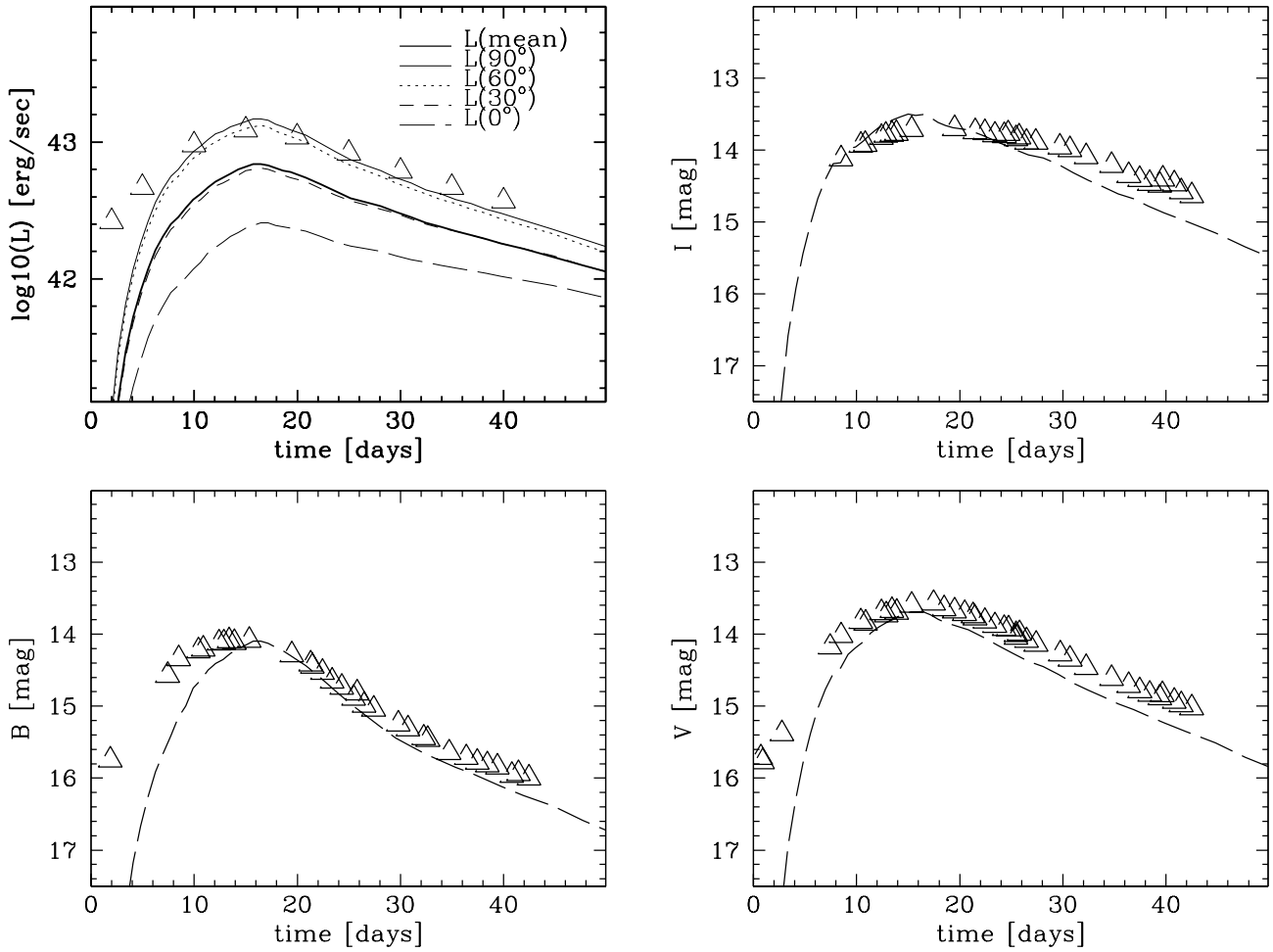

FIG. 8.—Comparison of bolometric and broadband light curves as observed for SN 1998bw with those of an oblate ellipsoid seen at high angle with respect to the equator. The theoretical light curves have been reddened corresponding to $A_V = 0.2$ mag.

is clumpy, the mean diffusion timescales would be reduced since the energy transport tends to occur through the regions with lower optical depth. Both of these effects would result in a faster rise of the early light curves.

The decline after maximum is slightly too steep in the models both in the bolometric and broadband light curves. This is likely to be related to the energy generation in the envelope by γ-ray deposition or to the change in the escape probability of low energy photons. The decline rate after maximum light might be affected by several factors. The instantaneous radioactive decay input becomes a more dominant contribution at later times as previously stored thermal energy is dissipated. The decline rate immediately after peak will thus be reduced by increasing the amount of radioactive ^{56}Ni. By day 40–50, the diffusion timescales are only a few days. The increase of ^{56}Ni needed to fill the gap between the bolometric (and broadband) light curves is estimated to be $\approx$40%. Another (related) possibility is suggested by Figure 5. The escape probability for γ-rays increases rapidly between day 20 and 80. Variations in model parameters may shift the time of this rapid change to earlier or later epochs. The first option seems to be unlikely as it implies that the total luminosity at later times should mainly be provided by the energy deposition due to positrons. This would require an increase of the ^{56}Ni mass by a factor of $\approx$30, so this option is excluded. A decrease in the rate of change of the γ-ray escape probability would also flatten the light curve. This can be achieved by a modification of the structure of the inner layers of the ejecta that determine the escape probability. Either a reduction of the expansion velocity of the inner layers or a steepening of the density profile there would give a slower decline from maximum. Both are expected for strongly aspherical explosions because the energy deposition will not be at the inner edge but distributed over a larger radial distance. In principle, late time observations of the width of ^{56}Co lines and the very late bolometric light curve could be used to distinguish the different options. In light of our approximations, we have chosen to forgo the exercise of further fine-tuning the models in favor of future, more self-consistent hydrodynamic and radiative transfer calculations.

5. DISCUSSION AND CONCLUSIONS

We have presented light curves for aspherical models of SNe Ic. The size of the asphericity was chosen to match the observed polarization in core-collapse supernovae with small or negligible H-rich envelopes. For appropriate axis ratios of about 2, we find that the apparent luminosity varies from equator to pole by roughly 2 mag for both oblate and prolate structures. The effect of asphericity may therefore be as important as the total amount of ^{56}Ni.

Asphericity may be produced by rapid rotation of the progenitor in a close binary system or by aspherical explo-

sions. An example of the latter would be a greater energy release in the polar direction. Such an asymmetric energy input will produce oblate density structures. More energy release into the equatorial direction will cause prolate structures. To result in a final asymmetry in the homologous phase with an axis ratio ~ 2 sufficient to account for the polarization of SN Ic and the luminosity of SN 1998bw requires a factor of 6 more kinetic energy per unit solid angle in the polar direction compared to the equatorial direction. Since asphericity tends to be smoothed out during the acceleration phase prior to homologous expansion, this may imply a much larger initial anisotropy in the energetics of the core-collapse process itself.

Because we do not know the mechanisms of core collapse or the production of asymmetries, it is important to look for statistical properties of the different configurations. For oblate geometries, high luminosity should be correlated with low polarization and, depending on the excitation, with high expansion velocities implied by strong lines, whereas the opposite trends are expected for oblate structures.

Our estimates of the expansion velocities implied by lines should be taken with a grain of salt. SNe Ic spectra are line-dominated and, consequently, have no well-defined photosphere. The spectral features are formed by strong lines with a very high optical depth above the region where the mean opacity becomes close to unity.

One requirement to form a line at a given Doppler shift, v_D, is that some material of the relevant composition move with the corresponding velocity. The maximum Lagrangian velocity thus provides an upper limit for v_D. On the other hand, the region where the mean opacity becomes close to unity provides the lower limit for v_D. In the current models at maximum light, these velocities differ by a factor of ≈ 3 and $v(\Theta)$ changes from prolate at the photosphere to slightly oblate at the highest velocities. A solution of the problem of spectral formation thus requires detailed NLTE calculations. The spectrum will depend on the excitation mechanisms and hence on the angular dependence of the outward mixing of radioactive material.

We have shown that the high apparent luminosity of SN 1998bw may be understood within the framework of "classical" SNe Ic. Even with our current model, SN 1998bw remains at the bright end of the scale. We note that the luminosity of SN 1998bw may be uncertain by a factor of $\pm 60\%$ because of non-Hubble motion within the cluster and uncertainties in the Hubble constant and the reddening. For a model with an ejected mass of the C/O envelope of 2 $M_\odot$, an explosion energy of 2×10^{51} ergs, and an ejected ^{56}Ni mass of 0.2 $M_\odot$, both the bolometric and broadband light curves are rather well reproduced by an oblate ellipsoid with an axis ratio of 0.5 that is observed within 30° of the symmetry axis. This angle for the line of sight is consistent with the low (but still significant) polarization observed for SN 1998bw. In a Lagrangian frame, the polar expansion velocity is a factor of 2 larger than the mean velocity. This is also in agreement with the rather large expansion velocities seen in SN 1998bw. More quantitative estimates require detailed NLTE calculations for the optically thin region. Within our framework, prolate geometries can be ruled out from the polarization.

Woosley et al. (1999) have analyzed the possibility of γ-ray bursts in the framework of spherical models. Even with their explosion energies of more than 20 foe they showed that the γ-ray burst associated with SN 1998bw/GRB 980425 cannot be explained by the acceleration of matter to relativistic speeds at shock breakout. In our picture, the specific energy released in the polar region is comparable to that in Woosley's models even though the total energy is much less. This asymmetry in the energy distribution, however, corresponds to the homologous phase. The initial anisotropy in the energy distribution associated with shock breakout is expected to be significantly higher. We note that the high-energy densities in a small amount of mass near the axis could give high entropy in the inner regions and hence conditions of high entropy that are conducive to the formation of an *r*-process.

Detailed studies of aspherical explosions, light curves, and NLTE spectral synthesis will be done in the future to provide a clear separation of the different scenarios. Note that the time evolution of P depends on the result of the hydrodynamical structure, i.e., its geometry, the variation of the shape of the "photosphere" in time, and the change of the optical depth (see above and Höflich 1995b). The list of possible improvements to the current models is long and includes stellar structures for rapidly rotating cores, aspherical core collapse, and, in light of the dependence of the postmaximum decline on the γ-ray escape probability, a more realistic distribution of the explosion energy in the inner layers.

We have shown that SN 1998bw may be understood within the framework of classical core-collapse supernovae rather than as a "hypernova." In light of the reasonable fits of Iwamoto et al. (1998), however, we cannot rule out the hypernova scenario. There may be ways to discriminate the hypernova scenario from our asymmetric models. Aspherical explosions with kinetic energy of 1 foe are expected to produce much smaller velocities for the inner ^{56}Ni-rich layers than hypernova models with $\gtrsim 20$ foe. The asymmetric models predict rather low expansion velocities ($v_{exp} \lesssim 7000$ km s^{-1}) for ^{56}Co that could be observed in late-time spectra. Another difference is the polarization. This is not predicted in the current spherically symmetric hypernova models of Iwamoto et al. (1998) and Woosely et al. (1999), but they could presumably be rendered asymmetric in some way. With lower ejecta mass, the models we present here predict that the polarization should start to decline as the envelope becomes transparent at $\approx$ day 60–80. The more massive hypernova models would probably be consistent with a later phase of transparency and hence a later phase of declining polarization. The current models and the hypernova models also make substantially different predictions for the amount of ejected. If SN 1998bw decays at the timescale corresponding to ^{56}Co, then photometric observations of the slope of the tail should discriminate between the two classes of models.

In this paper, we have not directly addressed the broader issue of the possible connection of supernovae and γ-ray bursts. The open questions are whether SN 1998bw is identical with GRB 980425 and whether we expect a correlation between SNe Ib/c and γ-ray bursts. Wang & Wheeler (1998) concluded that a connection of SNe Ib/c to γ-ray bursts could not be ruled out. Kippen et al. (1998) found no evidence for a connection between supernovae and γ-ray bursts, and Graziani, Lamb, & Marion (1998) concluded that not all SNe Ib/c could be associated with γ-ray bursts although a fraction might be. With the small sample of SNe Ib/c and partial sky coverage, it will be difficult to resolve

this issue with statistics alone. Neither the hypernova models nor the current models can directly produce a γ-ray burst by shock acceleration (Iwamoto et al. 1998; Woosley et al. 1999; see above). If some of the γ-ray bursts at large redshifts are driven by supernovae, then the associated energy flow must be strongly collimated, and aspherical core collapse may be a natural way to produce such jets.

The basic purpose of this paper is to underline the fact that asymmetries must be taken into account in a complete consideration of core-collapse supernovae, of SN 1998bw in particular, and, by extension of γ-ray bursts.

We thank Ken Nomoto for providing us with the broad-band light-curve data in digital form. This research was supported in part by NSF grant AST 95-28110, NASA grant NAG 5-2888, and a grant from the Texas Advanced Research Program.

REFERENCES

Boella, G., Butler, R. C., Perola, G. C., Piro, L., Scarsi, L., & Bleeker, J. A. M. 1997, A&AS, 122, 299
Castor, J. I. 1974, MNRAS, 169, 279
Chevalier, R. A., & Soker, N. 1989, ApJ, 341, 611
Collela, P., & Woodward, P. R. 1984, J. Comput. Phys., 54, 174
Clochiatti, A., & Wheeler, J. C. 1997, in Thermonuclear Supernovae, ed. P. Ruiz-Lapuente, R. Canal, & J. Isern (Dordrecht: Kluwer), 863
Cunto, W., & Mendoza, C. 1992, Topbase 0.7, IBM Venezuela Scientific Center
Duus, A., & Newell, B. A. 1977, ApJS, 35, 309
Fishman, G. J., et al. 1993, A&AS, 97, 17
Galama, T. J., et al. 1998, Nature, submitted (astro-ph/9806175)
Graziani, C., Lamb, D. Q., & Marion, G. H. 1998, ApJ, submitted (astro-ph/9810374)
Höflich, P. 1991, A&A, 246, 481
———. 1995a, ApJ, 440, 821
———. 1995b, ApJ, 443, 89
Höflich, P., & Khokhlov, A. 1996, ApJ, 457, 500
Höflich, P., Khokhlov, A., & Müller, E. 1992, A&A, 259, 243
Höflich, P., Müller, E., & Khokhlov, A. 1993, A&A, 268, 570
Höflich, P., Wheeler, J. C., Hines, D., & Trammell, S. 1995, ApJ, 459, 307
Höflich, P., Wheeler, J. C., & Thieleman, F. K. 1998, ApJ, 495, 617
Iwamoto, K., Nomoto, K., Höflich, P., Yamaoka, H., Kumagai, S., & Shigeyama T. 1994, ApJ, 437, L115
———. 1998, Nature, 395, 672
Jeffery, D. J. 1991, ApJ, 375, 264
Kay, L. E., Halpern, J. P., Leighly, K. M., Heathcote, S., & Magalhaes, A. M. 1998, IAU Circ. 6969
Kippen, R. M., et al. 1998, ApJ, 506, L27
Kulkarni, S. R., et al. 1998, Nature, 395, 663
Kurucz, R. L., & Bell, B. 1995, CD-ROM 23, Atomic Line Data (Cambridge: Smithsonian Astrophys. Obs)
Méndez, M., Clochiatti, A., Benvenuto, O. G., Feinstein, C., & Marraco, H. G. 1988, ApJ, 334, 295
Mihalas, D. 1978, Stellar Atmospheres (San Francisco: Freeman)
Nomoto, K., & Hashimoto, M. 1988, Phys. Rep., 163, 13
Paczyński, B. 1997, ApJ, 494, L45
Patat, G., & Piemonte, A. 1998, IAU Circ. 6918
Schlegel, D. J., Finkbeiner, D. P., & Davis, M. 1998, ApJ, 500, 525
Schmidt, B., et al. 1997, AJ, 107, 1444
Sobolev, V. V. 1957, Soviet. Astron., 1, 297
Steinmetz, M., & Höflich, P. 1992, A&A, 257, 641
Tinney, C., Stathakis, R., Cannon, R., & Galama, T. J. 1998, IAU Circ. 6896
Trammell, S. R., Hines, D. C., & Wheeler, J. C. 1993, ApJ, 414, L21
Tran, H. D., Filippenko, A. V., Schmidt, G. D., Bjorkman, K. S., Jannuzi, B. T., & Smith, P. S. 1997, PASP, 109, 489
Wang, L., & Wheeler, J. C. 1998, ApJ, 504, L87
Wang, L., Wheeler, J. C., & Höflich P. 1998, in SN1987A: Ten Years Later, ed. M. M. Phillips & N. B. Suntzeff (Dordrecht: Kluwer), in press
Wang, L., Wheeler, J. C., Li, Z. W., & Chlochiatti, A. 1996, ApJ, 467, 435
Woosley, S., Eastman, R., & Schmidt, B. 1999, ApJ, 516, 788